

The North Alabama Lightning Mapping Array: Recent Severe Storm Observations and Future Prospects

S. J. Goodman^{1*}, R. Blakeslee¹, H. Christian¹, W. Koshak¹, J. Bailey², J. Hall², E. McCaul²,
D. Buechler², C. Darden³, J. Burks³, T. Bradshaw³, P. Gatlin²

NASA Marshall Space Flight Center¹, Global Hydrology & Climate Center², and National
Weather Service Forecast Office³, National Space Science and Technology Center,
Huntsville, AL, 35805

*Corresponding author. Mailing address: 320 Sparkman Drive, Huntsville, AL, 35805, USA,
Tel.: +1-256-961-7891; fax +1-256-962-7979; e-mail: steven.goodman@nasa.gov (Steven
Goodman).

Revised May 6, 2004.

ABSTRACT

The North Alabama Lightning Mapping Array became operational in November 2001 as a principal component of a severe weather test bed to infuse new science and technology into the short-term forecasting of severe and hazardous weather, principally within nearby National Weather Service forecast offices. Since the installation of the LMA, it has measured the total lightning activity of a large number of severe weather events, including three supercell tornado outbreaks, two supercell hailstorm events, and numerous microburst-producing storms and ordinary non-severe thunderstorms. The key components of evolving storm morphology examined are the time rate-of-change (temporal trending) of storm convective and precipitation characteristics that can be diagnosed in real-time using NEXRAD WSR-88D Doppler radar (echo growth and decay, precipitation structures and velocity features, outflow boundaries), LMA (total lightning flash rate and its trend) and National Lightning Detection Network (cloud-to-ground lightning, its polarity and trends).

For example, in a transitional season supercell tornado outbreak, peak total flash rates for typical supercells in Tennessee reached 70-100 min^{-1} , and increases in the total flash rate occurred during storm intensification as much as 20-25 min prior to at least some of the tornadoes. The most intense total flash rate measured during this outbreak (over 800 flashes min^{-1}) occurred in a storm in Alabama. In the case of a severe summertime pulse thunderstorm in North Alabama, the peak total flash rate reached 300 min^{-1} , with a strong increase in total lightning evident some 9 min before damaging winds were observed at the surface. In this paper we provide a sampling of LMA observations and products during severe weather events to illustrate the capability of the system, and discuss the prospects for improving the short-term forecasting of convective weather using total lightning data.

Keywords: Total lightning activity; Thunderstorms; Severe weather applications; Forecasting

1. INTRODUCTION

The North Alabama 3-D VHF regional Lightning Mapping Array (LMA; Rison et al. 1999; Krehbiel et al. 2000; Thomas et al. 2000; Goodman et al. 2002) consists of ten VHF receivers deployed across northern Alabama and a base station located at the National Space Science and Technology Center (NSSTC), which is on the campus of the University of Alabama in Huntsville. The LMA system locates the sources of impulsive VHF radio signals from lightning by accurately measuring the time that the signals arrive at the different receiving stations. Each station records the magnitude and time of the peak lightning radiation signal in successive 80 μs intervals within a local unused television channel (channel 5, 76-82 MHz in our case). Typically hundreds of sources per flash can be reconstructed, which in turn produces accurate 3-dimensional lightning image maps (nominally <50 m error within 150 km range). The data are transmitted back to a base station using 2.4 GHz wireless Ethernet data links and directional parabolic grid antennas. There are four repeaters in the network topology and the links have an effective data throughput rate ranging from 600 kbits s^{-1} to 1.5 Mbits s^{-1} .

In real-time operation, faster data processing is needed without compromising the high flash detection efficiency of $\sim 100\%$. To accomplish this, the data at each station are decimated moderately by identifying the peak pulse in a larger 500 μs window (2000 samples s^{-1}). However, the full resolution data are still archived on site and brought back via the links (and by the scientific staff) during periods of inactive weather. The decimation allows tens of sources from each flash to be reconstructed, which is sufficient for the total flash rate of each storm to be computed reliably in near real-time.

Key objectives of our research investigations using the total lightning data obtained by the LMA are:

- * Identification of intensifying and weakening storms using the time rate-of-change of total flash rate;
- * Evaluation of the potential of total flash rate trend to improve severe storm probability of detection (POD) and lead time (Williams et al. 1999).

In this paper, we focus on two contrasting severe weather events; one an isolated warm-season microburst-producing pulse severe thunderstorm on 18 August 2002, and the second a major outbreak of tornadic supercell thunderstorms on 10-11 November 2002. We present data covering the entire life cycle of the pulse storm, but only an overview of the complexities of the tornadic supercell outbreak, with details on only two of the supercells.

2. METHODOLOGY

Total lightning data were obtained from the LMA network, while the cloud-to-ground (CG) lightning data were obtained from the National Lightning Detection Network (NLDN; Cummins et al. 1998). Both types of lightning data were analyzed over a 460 km x 460 km region centered over the LMA network, whose centroid is at 34.724N, 86.645W. Doppler radar measurements were obtained from the National Weather Service WSR-88D radar located at Hytop, Alabama (KHTX). The severe weather events associated with each storm were obtained by comparing the times and locations of the events reported in the National Climatic Data Center publication "Storm Data" with radar reflectivity plots.

The various cells were identified and tracked subjectively by plotting maps of the vertically integrated LMA source density fields, gridded on a 2 km × 2 km horizontal mesh, in ~5 min intervals defined by KHTX volume scan start times. For each storm cell of interest, a bounding box of time-varying size not less than 0.2° × 0.2° in latitude and longitude was then drawn around the cell's source density maximum; this included most of the sources associated

with the core of the thunderstorm cell, with minimal interference from nearby competing cells. Care was taken to ensure that a given storm's bounding box never included any of the high source-density core region of an adjacent cell.

We used temporal and spatial clustering criteria of 0.3 s and 2.0 km, respectively, to partition VHF source sequences into flashes, but we used a relaxed spatial clustering criterion at ranges beyond 50 km from the network center to account for source location uncertainties that increase with range. These time clustering criteria are similar to those that have been used in other similar analyses (Boldi et al. 1998; Williams et al. 1999, Christian et. al., 2000), but the spatial criteria at close range from the network have been tightened somewhat relative to the earlier studies, in order to provide better resolution of individual flashes in high flash-rate storms. However, at longer ranges, the flash spatial clustering appears to be dominated by source location errors that increase quadratically with range, which limit our ability to perform accurate analyses of the spatial structure of flashes at ranges greater than about 160 km. It is at this latter range that the range location uncertainty begins to be comparable to the typical spacing between storm cells. In this paper, we restrict our analyses to storms observed at ranges <160 km from the network center. Once flashes were defined by the clustering algorithm, the LMA-derived total flash counts for each cell were tallied by counting all distinct flashes having sources that fell within that cell's bounding box.

It is difficult to validate the accuracy of any flash algorithm when studying high-flash rate storms such as the ones described in this paper, because algorithm output is somewhat sensitive to the temporal and spatial clustering criteria employed, particularly the empirically-derived estimate of the coefficient of the quadratic function describing the range dependence of range location error. However, our estimates of the quadratic range dependence of this source location error have been assigned a cautiously large coefficient here, so that if our flash counts contain any bias errors, the counts are likely to be too small. Ongoing analysis of

LMA source location errors (see, e.g., Koshak et al. 2004), will help us more accurately determine the ultimate usable range of the LMA data.

Using a procedure analogous to that used in our LMA total lightning flash tally, we then additionally proceed to count, for each radar time interval, the number of NLDN-observed CG flashes (with distinct counts for positive and negative polarities), KHTX-derived storm top heights, Doppler velocity information on rotational or divergent flow features, maximum radar reflectivity values, and the maximum Vertically Integrated Liquid (VIL; Greene and Clark 1972) associated with each storm. The bounding boxes used for evaluation of the radar-derived parameters were the same as for total lightning; this ensures that correct and representative values were obtained. For rotational velocity and maximum reflectivity, we recorded the data in the form of time-varying vertical profiles. Rotational shear was computed at each radar scan time and elevation angle as $(V_{out} - V_{in})/d$, where V_{out} and V_{in} are the maximum inbound and outbound Doppler velocities, and d is the distance between the velocity couplet. The velocity differential was computed at each radar scan time at the lowest elevation angle (0.5°) as the maximum difference between the outbound and inbound velocity values along individual radials, and represents a measure of storm outflow divergence. For reflectivity, maximum values as a function of altitude were obtained by interpolating the raw reflectivity values to a 1km x 1km x 1km Cartesian grid and extracting the maximum value within each bounding box at each 1 km vertical increment. This maximum reflectivity was only computed when the cell was within 125 km of KHTX. For the CG flash analysis, positive-polarity CG flashes having peak currents less than 10 kA were assumed to be misidentified intracloud flashes, as recommended by Cummins et al. (1998).

In operational mode, a storm cell identification and tracking algorithm updates the storm characteristics and position with each volume scan, and a nearest neighbor spatial-temporal clustering algorithm associates the NLDN CG flashes and LMA total lightning

flashes with the various cells to permit trending of radar-derived storm characteristics and lightning rate. The time rate-of-change of storm characteristics and life-cycle trending are accomplished in real-time through the second generation Linked Information System Data Access and Dissemination (LISDAD II) system, initially developed in 1997 through a collaboration among NASA/MSFC, MIT/Lincoln Lab and the Melbourne, Florida NWS Office (Boldi et al. 1998). LISDAD II is now a distributed decision support system with a JAVA-based display application that allows anyone, anywhere, to track individual storm histories within the southeastern United States (U. S.).

A 3-D gridded total lightning source data set is also generated from the decimated LMA VHF data at 2 km horizontal and 1 km vertical resolutions within a 460 km x 460 km domain having 17 km vertical levels; these data are updated every 2 min. These data provide essentially full coverage of the Huntsville and Nashville NWS warning areas, as well as partial coverage of the warning areas of five other NWS offices. The NWS Local Data Acquisition and Dissemination (LDAD) system ingests these near real-time VHF source density grids, which are then provided to the Advanced Weather Information Processing System (AWIPS) forecaster workstation that is used to display varied weather data and issue forecasts and warnings. The availability of LMA data within the AWIPS workstation enables forecasters for the first time to operationally integrate total lightning measurements with radar, satellite, and other weather data. Forecasters can interrogate the data on any of the 17 horizontal levels or examine the cumulative source density map that includes all levels. Forecasters can also readily dither between NEXRAD and total lightning maps and loop multiple frames to enhance situational awareness during severe weather episodes. The total lightning products are automatically updated on the forecasters' workstation. In this way, the forecaster can optimally evaluate the added value of total lightning data within the forecast and warning decision-making process.

It is important to understand the timeline that describes when the various lightning and radar data products are available for inspection and analysis by nowcasters at NWS offices. Low-level reflectivity structures are presented on-screen within 30 s of the start of a radar volume scan, while echo tops and vertically integrated liquid (VIL) are not available until the end of a volume scan. The maximum latency of each product is equal to the duration of a volume scan, typically 5-6 min. The LMA source data are provided in gridded form every 2 min, with a latency of at most 2 min. Thus, in all time series graphics shown below, we have tallied statistics in temporal bins equal in duration to the radar volume scans, but have plotted echo tops and VIL at the end of the radar volume scan time, and LMA total and NLDN CG lightning data delayed by 2 min relative to the radar scan start times. These delays and latency periods are tabulated for reference in Table 1. One of the chief advantages of the lightning data is the reduced latency of the data relative to the length of radar volume scan intervals.

3. RESULTS AND DISCUSSION

Since the inception of LMA operations in 2001 there has been an abundance of severe weather within the effective domain of coverage extending about 250 km in range from Huntsville, Alabama. For example, during 23-24 November 2001, total lightning measurements of a major tornado outbreak were obtained by the LMA in its first data acquisition effort (30 tornadoes in North Alabama). The single greatest tornado outbreak event of 2002 occurred on 10-11 November 2002, extending from the southeast U. S. into Ohio and Pennsylvania, with 32 confirmed tornadoes in the four-state area of Alabama, Mississippi, Tennessee, and Georgia alone. On 19 March 2003, ten tornadoes were reported in northern Alabama and southern Tennessee. Total lightning observations were obtained throughout the life cycles of many of these storms. Numerous summertime pulse thunderstorms, some severe, have also been observed by the LMA.

Observations from a summer pulse-type severe thunderstorm on 18 August 2002 and the outbreak of tornadic supercells beginning on 10 November 2002 serve to illustrate some of the variety of severe convective weather conditions documented by the LMA, and its utility in monitoring total lightning trends that often portend severe weather occurrences.

3.1 Severe Summertime Pulse Storm

At approximately 2020 UTC 18 August 2002, the first updraft of what would become a pulse storm complex consisting of a clustered series of multicell updrafts erupted over Huntsville. As is typical of afternoon summertime pulse storms in this region, winds were light and the vertical shear weak, and the storm moved little during its lifetime. As Fig. 1 shows, the first updraft rapidly intensified, producing an echo top of 16 km and a VIL of 50 kg m⁻², and generating LMA-derived total lightning flash rates exceeding 100 min⁻¹ by 2058 UTC. NLDN indicates that by 2103 UTC, this storm was producing a transient peak of 5 cloud-to-ground flashes min⁻¹. By 2108 UTC, total flash rates, after holding steady briefly, began to increase rapidly again, apparently in response to a second, even stronger updraft pulse. CG rates subsequently trended upward, achieving a peak of more than 6 flashes min⁻¹ by 2120 UTC, shortly before the total flash rate reached its overall storm peak of more than 300 flashes min⁻¹. At around this time, severe downburst winds began to be noted in western portions of Huntsville, with NSSTC's roof anemometer recording a 34 m s⁻¹ gust at 2117 UTC, along with heavy rain falling at the one-minute rate of 150 mm hr⁻¹. Considerable tree damage and local flooding occurred in the vicinity of the downburst, and four houses were set on fire in the area by CG lightning strikes. Fig. 2 provides maps of (a) reflectivity at 2115 UTC, near the time of peak storm intensity, and (b) VHF source density from 2116:12-2121:11 UTC. The isolated nature of this intense storm within the field of widespread storms is evident in both radar and total lightning data. We find in this case, as in many others, that

the LMA source density maps can act as a surrogate for radar reflectivity in locating the positions of intense storm cells.

Additional radar analyses (Fig 2c) indicate that this multicell pulse storm complex achieved maximum reflectivities of greater than 60 dBZ, at altitudes up to 7 km, around the time of the severe weather. The peak low-level radial velocity difference observed by the radar, however, was only 17 m s^{-1} , much smaller than the peak gust observed at NSSTC. The failure of the radar to measure accurately the actual near-surface flows in the downburst likely owes to several factors: the shallowness of the divergent flow relative to the radar beamwidth; the placement of the radar on a mountaintop with several small mountain ranges lying between the radar and the Huntsville city area, and possibly the occurrence of the strongest surface winds in an asymmetric pattern, along directions nearly perpendicular to the radar beam. Experience in the Tennessee Valley region has shown, however, that even the observed 17 m s^{-1} divergent velocity difference is suggestive of potentially damaging downburst winds.

Later, after 2144 UTC, the LMA total lightning flash rate decreased rapidly, the radar reflectivity began to weaken, and the storm began to dissipate. Both CG and total lightning data provided advance indications of the impending severe weather, with significant upward trends in flash rates commencing near 2108 UTC as the second updraft pulse began to mature. Although the NLDN-derived CG rate peaks for this updraft pulse prior to the LMA-derived total flash rate, the upward trend in the total flash rate beginning at 2108 UTC gives a clearer early indication of impending storm severity than does the NLDN trend. Such trends in total flash rate and source counts are probably an indication of updraft intensity changes, which are closely linked with subsequent severe weather occurrences at the surface (Goodman et al. 1988; Williams et al. 1999).

3.2 Transitional Season Tornadic Supercell Outbreak

The tornadic supercells documented by the LMA on 10-11 November 2002 comprise a large and complex severe weather event that will be described in detail in a future paper. In this paper, the discussion is necessarily limited to a brief, general overview of the event, with detailed documentation of only two of the supercells. Regional maps of radar reflectivity and LMA-derived VHF source density at ~0100 UTC 11 November (Fig. 3) provide a snapshot of the outbreak when it was close to peak intensity. The WSI NOWRAD (TM) radar reflectivity composite, labeled with cell IDs, indicates the locations of the supercell storms that were within range of the LMA and that produced tornadoes just prior to or subsequent to 0100 UTC (Fig. 3a). The initiation time of the tornadoes and their Fujita F-scale ratings are summarized in Table 2. Cells B, D, E and G were located in Tennessee, while the remaining cells moved from Mississippi across Alabama. Some of these supercells produced tornado families. Most of the tornadoes in Tennessee existed for less than 15 min, but several very long-lived (>50 min duration) tornadoes occurred in Mississippi and Alabama from Cells I, J and L. The Tennessee storms developed late on the afternoon of 10 November, with the Mississippi storms developing later, as a strong capping inversion was gradually removed from north to south across the region.

The 3D LMA source density map, integrated over the 5-min interval 0100-0105 UTC, provides a snapshot synopsis of the convective vigor of the various storms (Fig. 3b). In this 5-min period there were 257945 VHF sources mapped, representing both intracloud (IC) and cloud-to-ground (CG) flashes. Of the 1017 CG flashes (indicated by the + and - symbols) observed by the NLDN, 660 were of negative polarity (-) and 357 of positive (+) polarity. However, only 65 of these positive CGs have peak currents >10 kA, likely indicating that the majority of the positives are misclassified intracloud flashes (Cummins et al. 1998). The East-West and North-South projections of the sources as a function of altitude point to the

most electrically active cells. Note that the lowest level of sources depicted in the E-W and N-S projections increases with height as a function of distance from the array because the LMA detects the VHF impulses along lines of sight, but Earth's curvature obstructs more and more of the lower parts of storms as range increases. Trending the amplitude and structure of these density maxima (as well as total flash rates) over time can provide the forecaster with nearly immediate awareness of the growth and decay of cells (Goodman et al. 2002); of updraft intensification, which could signal a growing likelihood for tornadogenesis (Williams et al. 1999); and of high risk areas for CG strikes.

Figure 4 provides an example of the detailed mapping and time-height depiction of flash events that the LMA is capable of. The figure shows a 90 s period of activity focused on Cell E (see Fig. 3 for overview at 0100 UTC) starting at 0026 UTC, ~26 min prior to the reported time of a killer F2 tornado touchdown. Note the presence of a prominent "lightning hole" near the southwest end of cell E. Such structures have been observed in other supercell storms, and are apparently closely associated with the storm's main updraft. Our initial impressions are that such lightning holes are nearly always associated with a bounded weak echo region and may help indicate the threat of severe weather. Cell E also had a clearly defined hook echo (not shown) at this time. The NLDN detected 3 negative and 5 positive polarity CGs during this same interval. The LMA-derived total flash rate for the storm was roughly 50 min^{-1} at this time, although the storm occasionally produced as many as $70 \text{ flashes min}^{-1}$. The individual total lightning flashes can be isolated and animated in time and space, providing tremendous detail on the evolution of each discharge and its relation to the reflectivity structure of the storm.

Fig. 5 contains time series plots of important storm parameters from tornadic cell G. This cell developed around 0030 UTC, and reached its first peak in intensity around 0050-0100 UTC. The total flash rates reach 100 min^{-1} at 0050, while the NLDN-derived CG flash

rate peaks first at 6 flashes min^{-1} at 0048 UTC, then at 8 flashes min^{-1} at 0103 UTC. However, Doppler-derived rotational shear (Fig 5d) in the cell's mesocyclone is unremarkable during this period. As with other tornadic supercells observed in this outbreak, tornadoes were seldom reported in association with the initial storm updraft burst, but occurred instead in association with subsequent bursts. Maximum cell reflectivity exceeds 60 dBZ near 7 km during this first updraft burst, which agrees well with the first peak in total flash rate. Most storm intensity parameters then show a weakening trend until about 0130 UTC, when a second updraft burst commences. Between 0133 and 0148 UTC, the total flash rate roughly doubles to 80 min^{-1} , while the CG rate peaks at 10 min^{-1} by 0158 UTC. As seen in the pulse storm described earlier, the total flash trend anticipates the CG trend by 5-10 min. Like the first updraft burst, reflectivity values aloft again increase with this second updraft burst, ultimately exceeding 65 dBZ. Unlike the first updraft burst, however, the reintensified updraft succeeds in generating a significant increase in low-level rotational shear, ultimately exceeding $30 \times 10^{-3} \text{ s}^{-1}$ after about 0140 UTC. This is followed by a significant decrease in CG flash rate just after 0158 UTC; the CG rate then remains low until 0208 UTC, when the cell produces its first tornado, an F2. This temporal pattern in CG rates may be an example of the lull in CG rates seen in Great Plains supercells during tornadogenesis, as documented earlier by MacGorman (1993). VIL also exhibits a significant increase during the time of this flash rate buildup, ultimately reaching 65 kg m^{-2} , a value achieved by many of the supercells in this outbreak. If taken as possible indicators of imminent tornadogenesis, the well-defined increases in the lightning and VIL parameters provide a potentially significant amount of warning lead time for this cell, but Doppler velocity data remained the best clue that rotation was insufficient for tornadoes during the first updraft burst.

It is interesting that the total flash rate for the 18 August 2002 pulse severe storm reached 300 min^{-1} , while the two transitional season tornadic supercells described here had

flash rates that reached only 70-100 min^{-1} . These rates should not, however, be taken as representative of all summertime pulse storms or tornadic supercells in the North Alabama area. The largest flash rate yet documented in North Alabama, more than 835 min^{-1} , occurred on 11 November 2002 in Cell I, which spawned a long-track killer F3 tornado before passing between Birmingham and Huntsville (see Fig. 3a). The complex structure and behavior of this very severe cell, which was evidently not representative of most storms in the 10-11 November 2002 outbreak, will be described in more detail in a future paper.

4. SUMMARY AND CONCLUSIONS

This paper presents severe storm observations from a summertime pulse storm case and from the 10-11 November 2002 tornado outbreak, and describes potentially useful operational products that can be derived using total lightning observations. For the 18 August 2003 severe summertime pulse thunderstorm in North Alabama, the peak total flash rate reached 300 min^{-1} , with a strong increase in total lightning evident some 9 min before damaging winds were observed at the surface. Both the total rate and CG flash rates increased as the storm intensified, but the increases were noted in the total lightning data prior to those in the CG data. Although radar indications also suggested the possible development of severe weather in this storm, the total flash rates were particularly large compared to standard radar parameter amplitudes, and could have provided a strong early indicator of possible severe weather to the warning decision process.

In the transitional season supercell tornado outbreak, peak flash rates for typical supercells in Tennessee reached 70-100 min^{-1} , and showed increases during storm intensification as much as 20-25 min prior to at least some of the tornadoes. CG rates also increased as much as 15-20 min prior to tornadoes, but in at least one case, showed a significant lull 5-10 min before the time of tornado touchdown. One of the larger, more

complex supercells in Alabama generated a peak total flash rate in excess of 800 min^{-1} , but this cell was not typical. Of course, it should also be noted that not all the large increases in storm total flash rate, or other radar or lightning parameters, were attended by subsequent tornadogenesis. In addition, for this very intense outbreak, radar and environmental indicators also pointed to the obvious tornadic potential of the storms, and the LMA data served primarily as a way of anticipating or confirming the need for warnings. In general, we maintain that the LMA lightning data should be used in conjunction with all other available data, including awareness of the storm environment, in making nowcasts of impending severe weather. It may well be that further research will show that the main benefit of the LMA data comes not during obvious severe weather outbreaks, but during the more common, marginal severe weather episodes, where the additional clues provided by the total lightning trends can better help distinguish which cells are about to cross the severe weather thresholds, and, equally important, which of the stronger cells are failing to do so. Total lightning data also allows forecasters to monitor and identify the locations of the most intense updrafts within convective lines.

The 2 min update cycle of the total lightning data (Table 1) allows forecasters to monitor storm intensity more often than by relying on radar parameters alone. By increasing the situational awareness of a storm's convective state, total lightning data increases the confidence of forecasters to act earlier on their warning decision. We have started to collect case studies of various convective situations and will present an analysis of them once the sample has grown large enough to provide statistically significant results.

ACKNOWLEDGMENTS

The authors thank NASA's Earth Science Enterprise (NASA UPNs 621-15-98, 621-82-80 and 622-41-02) and program manager James Dodge for support of this project. We also wish to acknowledge New Mexico Tech researchers (Paul Krehbiel, Ron Thomas, William Rison, Graydon Aulich, Timothy Hamlin, Jeremiah Harlin) for developing the LMA system and in helping us install and refine the North Alabama LMA.

NOWRAD (TM) is a registered trademark of WSI Corporation. The NOWRAD data and NLDN data were provided by the NASA Lightning Imaging Sensor (LIS) team via the Global Hydrology Resource Center (GHRC), through licensing agreements with WSI Corporation and Vaisala GAI, respectively.

REFERENCES

- Boldi, R., E. Williams, A. Matlin, M. Weber, S. Hodanish, D. Sharp, S. Goodman, and R. Raghavan, 1998: The design and evaluation of the Lightning Imaging Sensor Data Applications Display (LISDAD), Preprints, 19th Conf. Severe Local Storms, Minneapolis, MN, Amer. Meteor. Soc., Boston, MA, 631-634.
- Christian, H. J., R. J. Blakeslee, S. J. Goodman, and D. M. Mach (eds.), 2000: *Algorithm Theoretical Basis Document (ATBD) for the Lightning Imaging Sensor (LIS)*, 53 pp. NASA/Marshall Space Flight Center, Alabama. (available as http://eosps0.gsfc.nasa.gov/eos_homepage/for_scientists/atbd/viewInstrument.php?instrument=LIS, posted 1 Feb 2000).
- Cummins, K. L., M. J. Murphy, E. A. Bardo, W. L. Hiscox, R. B. Pyle, and A. E. Pifer, 1998: A combined TOA/MDF technology upgrade of the U. S. National Lightning Detection Network. *J. Geophys. Res.*, 103, 9035-9044.
- Goodman, S. J., D. E. Buechler, P. D. Wright, and W. D. Rust, 1988: Lightning and precipitation history of a microburst-producing storm. *Geophys. Res. Lett.*, 15, 1185-1188.
- Goodman, S. J., R. Blakeslee, H. Christian, D. Boccippio, W. Koshak, J. Bailey, J. Hall, M. Bateman, E. McCaul, D. Buechler, C. Darden, T. Bradshaw, and R. Boldi, 2002. Preprints, The North Alabama Severe Thunderstorm Observations, Research, and Monitoring Network (STORMnet), Preprints, 17th Int. Lightning Det. Conf. (ILDC-17), Tucson, AZ (electronic paper #9), CD-ROM available from Vaisala GAI.
- Greene, D. R., and R. A. Clark, 1972: Vertically integrated liquid water - A new analysis tool. *Mon. Wea. Rev.*, 100, 548-552.
- Krehbiel, P.R., R.J. Thomas, W. Rison, T. Hamlin, J. Harlin, and M. Davis, 2000: GPS-based mapping system reveals lightning inside storms. *EOS*, 81, 21-25.
- Koshak, W. J., R. J. Solakiewicz, R. J. Blakeslee, S. J. Goodman, H. J. Christian, J. M. Hall, J. C. Bailey, E. P. Krider, M. G. Bateman, D. J. Boccippio, D. M. Mach, E. W. McCaul, M. F. Stewart, D. E. Buechler, W. A. Petersen, and D. J. Cecil, 2004: North Alabama Lightning Mapping Array (LMA): VHF source retrieval algorithm and error analyses. *J. Atmos. Oceanic Tech.*, 21, 543-558.
- MacGorman, D. R., 1993: Lightning in tornadic storms: A review. in *The Tornado: Its Structure, Dynamics, Prediction, and Hazards*, C. R. Church, Ed., Amer. Geophys. Union, 173-182.
- Rison, W., R. J. Thomas, P. R. Krehbiel, T. Hamlin, and J. Harlin, 1999: A GPS-based three-dimensional lightning mapping system: Initial observations in central New Mexico. *Geophys. Res. Lett.*, 26, 3573-3576.
- Thomas, R. J., P. R. Krehbiel, W. Rison, T. Hamlin, D. Boccippio, S. Goodman, and H. Christian, 2000: Comparison of ground-based 3-dimensional lightning mapping observations with satellite-based LIS observations in Oklahoma. *Geophys. Res. Lett.*, 27, 1703-1706.
- Williams, E. R., B. Boldi, A. Matlin, M. Weber, S. Hodanish, D. Sharp, S. Goodman, R. Raghavan, and D. Buechler, 1999: The behavior of total lightning activity in severe Florida thunderstorms. *Special Issue of Atmos. Res.*, 51, 245-265.

FIGURE CAPTIONS

Fig. 1. Time series plots of KHTX radar-derived parameters and LMA-derived and NLDN-derived flash parameters for the entire lifetime of the pulse storm of 18 August 2002. (a) 30 dBZ echo top and VIL, and velocity difference between inbound and outbound Doppler velocity values (top); (b) LMA-derived total flash rate and NLDN-derived positive and negative flash rates (middle); (c) maximum reflectivity (dBZ) as a function of altitude (bottom). The "W" denotes the time of reported damaging surface winds.

Fig. 2. Maps of KHTX radar reflectivity and LMA lightning source density for 2115 UTC 18 August 2002, near the peak of the severe pulse storm in Huntsville (near center of domain). (a) WSI NOWRAD (TM) radar reflectivity mosaic at 2115 UTC, with pulse storm labeled "P" on its east side (top); (b) LMA source density integral from 2116:12-2121:11 UTC (bottom).

Fig. 3. Maps of regional radar reflectivity and lightning source density for a portion of the 10-11 November 2002 tornadic supercell event. (a) WSI NOWrad (TM) radar reflectivity mosaic at 0100 UTC 11 November 2002 (left). Tornadic cell IDs are indicated as in Table 2. (b) LMA 5-min (0100:27-0105:26 UTC) VHF source density with NLDN ground strikes (black, + for positive CG, - for negative CG) overlaid (right).

Fig. 4. Temporal integral of spatial locations of LMA VHF sources in cell E within a 90 s interval (0026:00-0027:30 UTC). Vertical projections above and right of base map shows VHF source density as a function of E-W and N-S distance versus altitude (km). NLDN ground strike polarity is also shown (triangle for negative CG, X for positive CG). A lightning hole is centered at $x=13$, $y=80$, near the main updraft of the cell.

Fig. 5. Time series plots of KHTX radar-derived parameters and LMA-derived and NLDN-derived flash parameters for the portion of the lifetime of Tornadic Cell G early on 11 November 2002. (a) echo top and VIL (top); (b) LMA-derived total flash rate and NLDN-derived positive and negative flash rates (second panel); (c) Doppler radar-derived maximum storm reflectivity (dBZ) as a function of altitude (third panel); and (d) Doppler radar-derived rotational shear (10^{-3} s^{-1}) as a function of altitude (bottom panel), the contours start at 0 s^{-1} and increase in $5 \times 10^{-3} \text{ s}^{-1}$ increments. The "V" markings denote the beginning times of reported tornadoes.

Table 1. Delays and Observation Intervals of Radar and Lightning Data Parameters Relative to the Start of a Radar Volume Scan.

Parameter	Time Available (min)	Observation interval (min)
Reflectivity	0.5	5.0-6.0
Echo Tops	5.0-6.0	5.0-6.0
VIL	5.0-6.0	5.0-6.0
LMA source density	0.0-2.0	2.0
NLDN data	0.0-0.5	flash

Table 2. Tornado chronology for 2300 UTC 10 November - 0300 UTC 11 November 2002 for the storm cells depicted in Fig. 3.

Cell ID	B	D	E	G	I	J	K	L*
Initiation time (UTC) and F#	2342/F1	2345/F2	0052/F2	0208/F2	0052/F3	0108/F3	0136/F1	0120/F1
	0108/F1			0230/F1		0215/F3		
	0131/F3			0246/F0				
	0154/F2							

* Supercell "L" went on to produce 7 more tornadoes after 0300 UTC 11 November 2002.

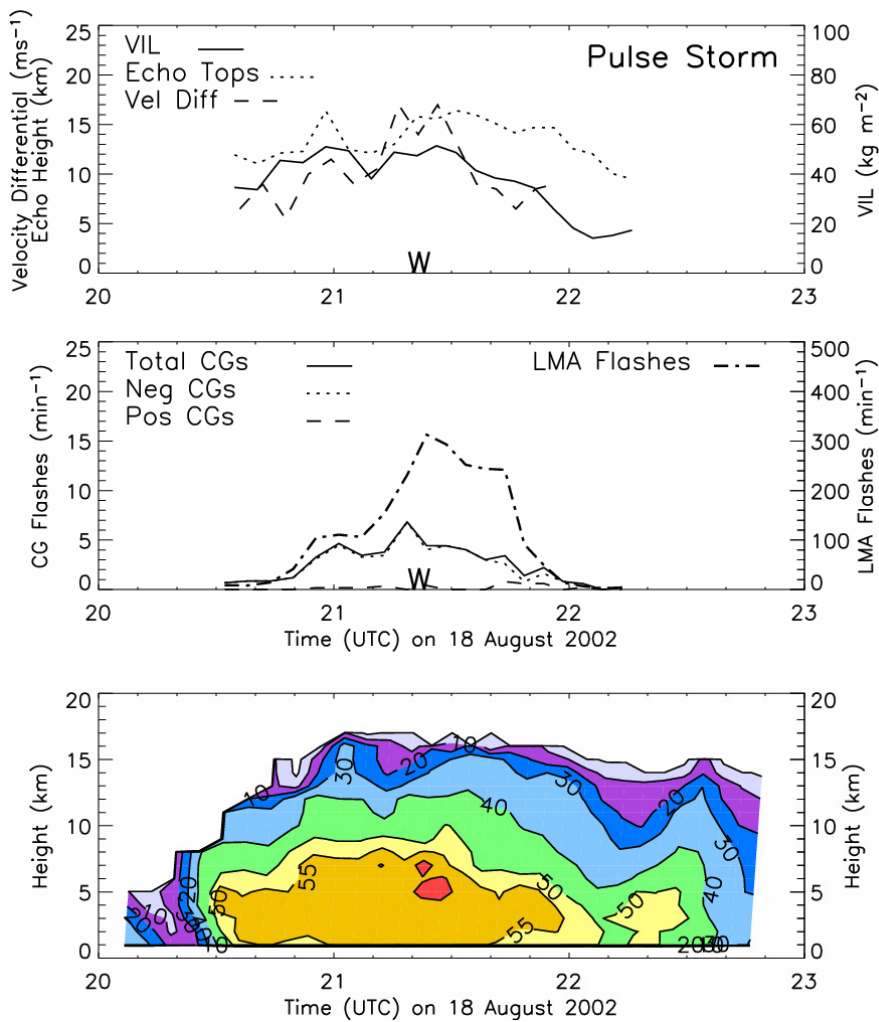


Fig 1. Time series plots of KHTX radar-derived parameters and LMA-derived and NLDN-derived flash parameters for the entire lifetime of the pulse storm of 18 August 2002. (a) 30 dBZ echo top, VIL, and velocity difference between inbound and outbound Doppler velocity values (top); (b) LMA-derived total flash rate and NLDN-derived positive and negative flash rates (middle); (c) maximum reflectivity as a function of altitude (bottom). The ‘W’ denotes the time of reported damaging surface winds.

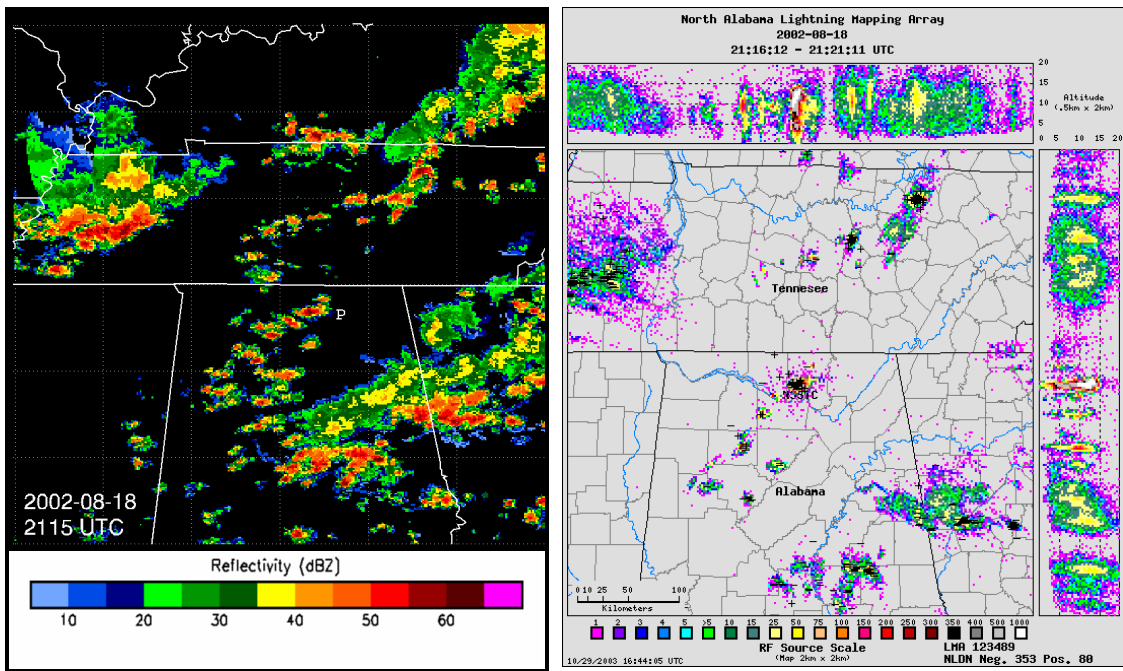


Fig. 2. Maps of KHTX radar reflectivity and LMA lightning source density for 2115 UTC 18 August 2002, near the peak of the severe pulse storm in Huntsville (near center of domain). (a) WSI NOWRAD (TM) radar reflectivity mosaic at 2115 UTC, with pulse storm labeled "P" on its east side (left panel); (b) LMA source density integral from 2116:12-2121:11 UTC (right panel).

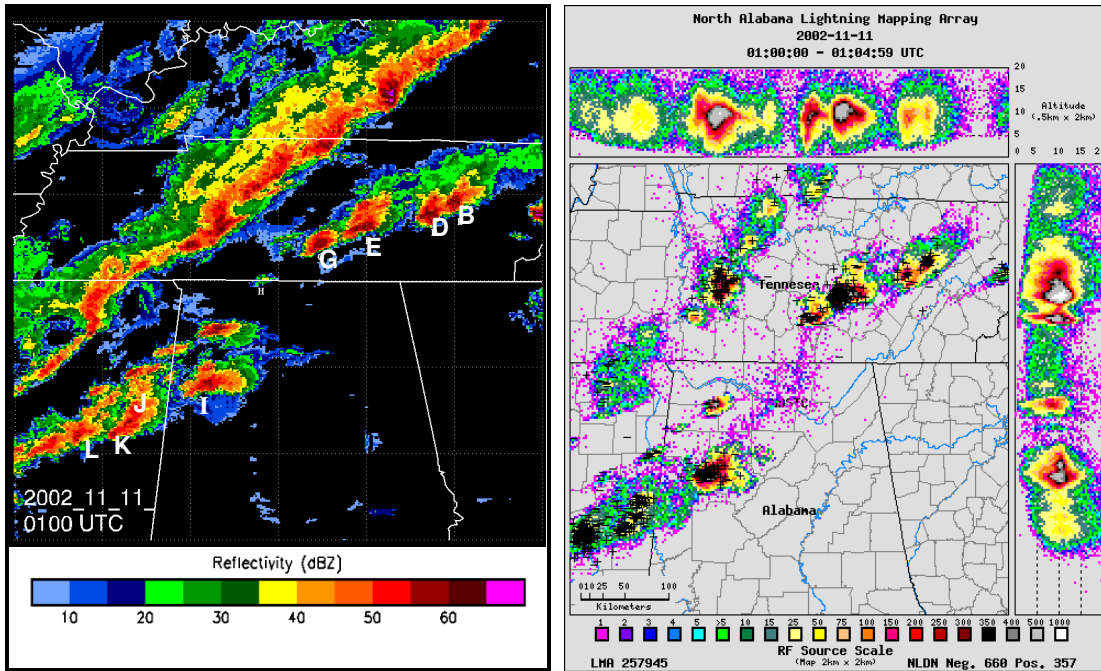


Fig 3. Maps of regional radar reflectivity and lightning source density for a portion of the 10-11 November 2002 tornadic supercell event. (a) WSI NOWRAD (TM) radar reflectivity mosaic at 0100 UTC 11 November 2002 (left panel). Tornadic cell IDs are indicated as in Table 2. (b) LMA 5-min (0100:27-0105:26 UTC) VHF source density with NLDN ground strikes (black, + for positive CG, - for negative CG) overlaid (right panel).

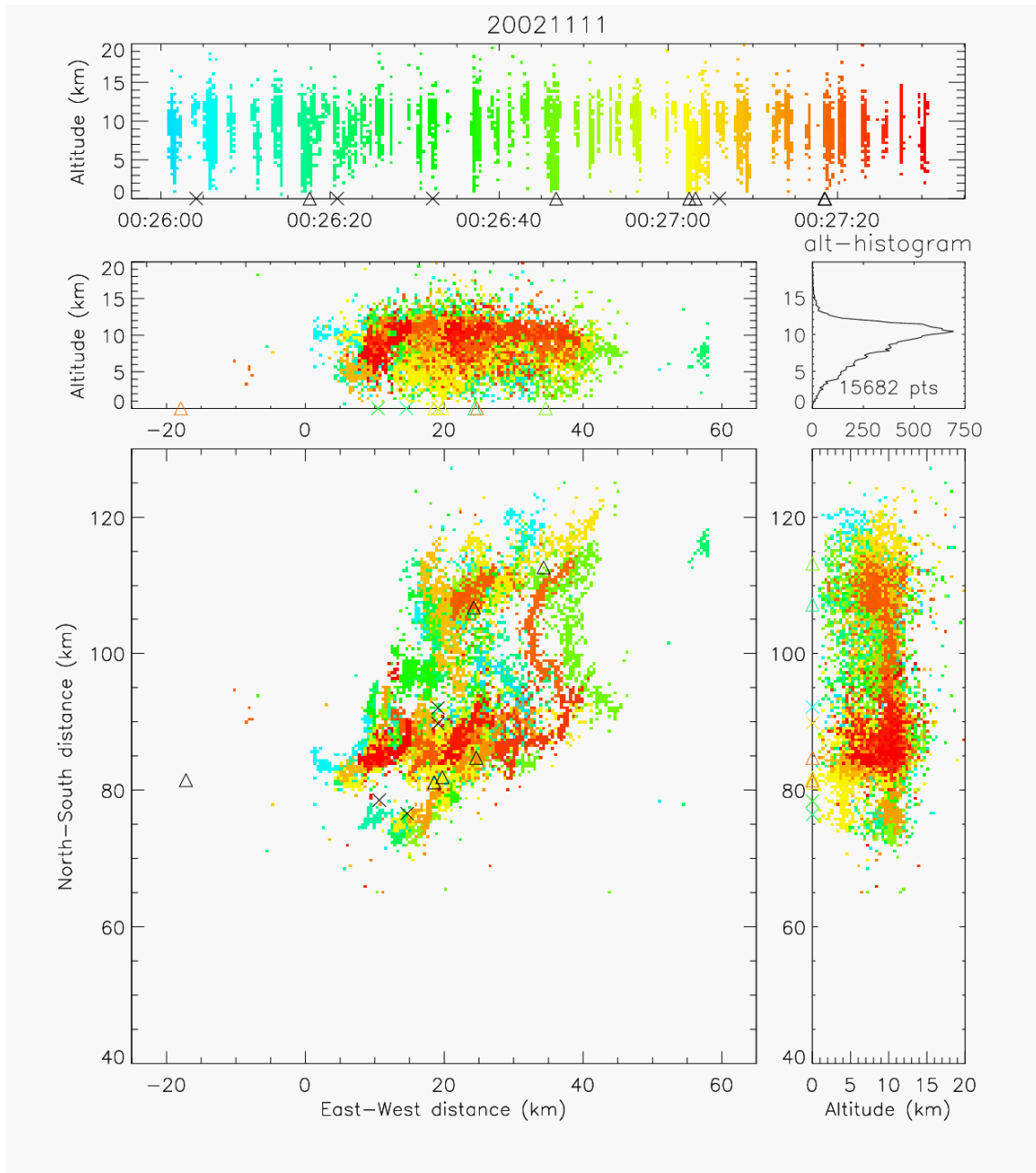


Fig. 4. Locations of LMA VHF sources in cell E within a 90 s interval (0026:00-0027:30 UTC). Vertical projections above and right of base map shows VHF source density as a function of E-W and N-S distance versus altitude (km). NLDN ground strike polarity is also shown (triangle for negative CG, X for positive CG). A lightning hole is centered at $x=13$, $y=80$, near the main updraft of the cell.

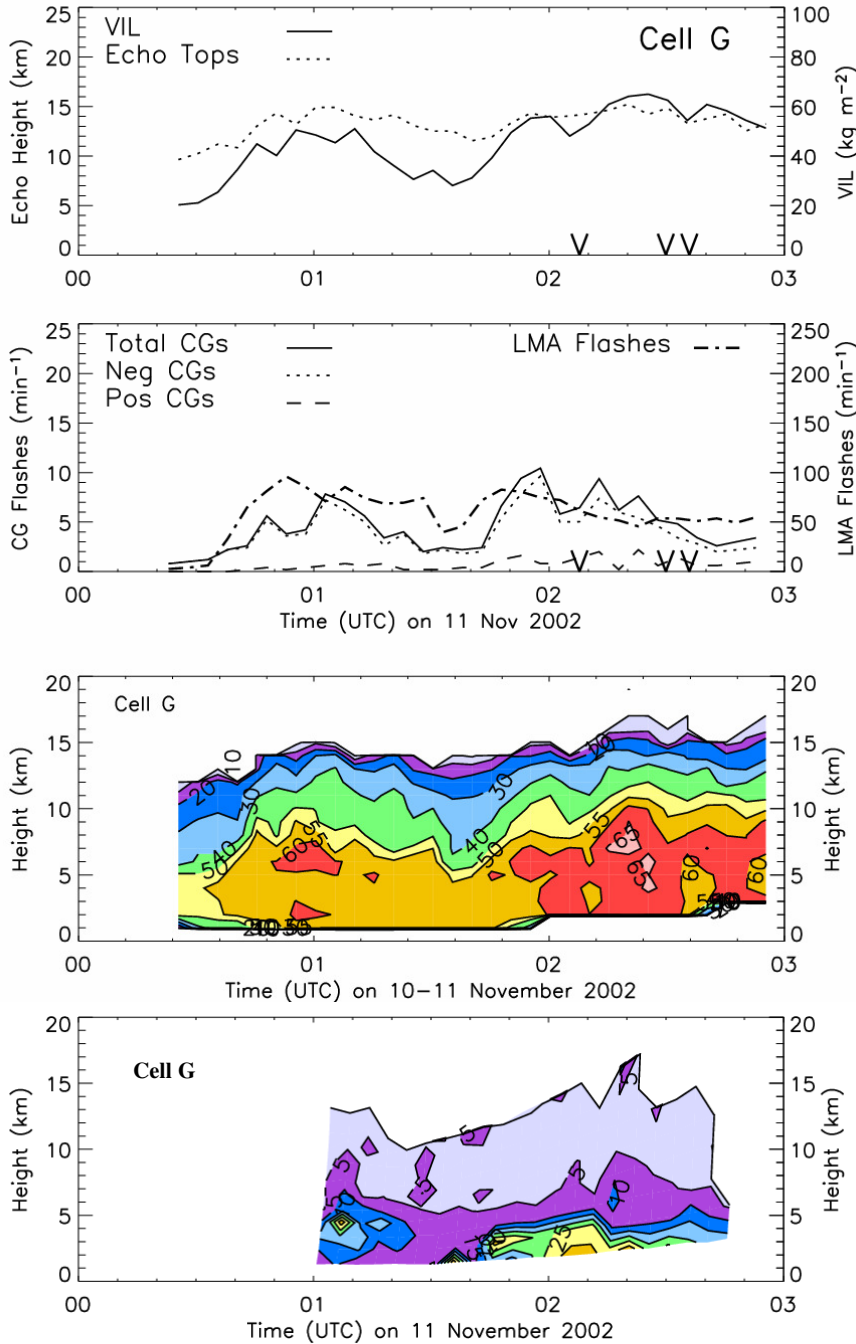


Fig. 5. Time series plots of KHTX radar-derived parameters and LMA-derived and NLDN-derived flash parameters for the portion of the lifetime of Tornadic Cell G early on 11 November 2002. (a) echo top and VIL (top); (b) LMA-derived total flash rate and NLDN-derived positive and negative flash rates (second panel); (c) Doppler radar-derived maximum storm reflectivity (dBZ) as a function of altitude (third panel); and (d) Doppler radar-derived rotational shear (10^{-3} s^{-1}) as a function of altitude (bottom panel), the contours start at 0 s^{-1} and increase in $5 \times 10^{-3} \text{ s}^{-1}$ increments. The "V" markings denote the beginning times of reported tornadoes.